

# THE ISRAELI EA-FEL UPGRADE TOWARDS LONG PULSE OPERATION FOR ULTRA-HIGH RESOLUTION SINGLE PULSE COHERENT SPECTROSCOPY

Y. Socol, A. Faingarsh, S. Peleg, M. Volshonok, A. Gover

Dept. of Physical Electronics – Faculty of Engineering, Tel Aviv University, Tel-Aviv, Israel

M. Einat, M. Kanter, B. Kapilevich, B. Litvak, Y. Lurie, Y. Pinhasi & A. Yahalom

Dept. of Electrical and Electronic Engineering – The College of Judea and Samaria, Ariel, Israel

## Abstract

The Israeli Electrostatic Accelerator FEL (EA-FEL) is now being upgraded towards long pulse (100 $\mu$ s) operation and ultra-high resolution ( $10^{-6}$ ) single pulse coherent spectroscopy. We present quantitative estimations regarding the applications of controlled radiation chirp for spectroscopic applications with pulse-time Fourier Transform limited spectral resolution.

The presentation provides an overview of the upgrade status: a new broadband low-loss resonator is being manufactured; multi-stage depressed collector is assembled.

## INTRODUCTION

The current status of the Israeli Electrostatic Accelerator FEL [1] (EA-FEL) allows the generation of pulses of tens microseconds duration. The mm-wave radiation is now transmitted to the user-center rooms, where it can be utilized, e.g., for THz spectroscopy [2].

The Israeli FEL is now being upgraded towards long pulse (100 $\mu$ s) operation and ultra-high resolution ( $10^{-6}$ ) single pulse coherent spectroscopy. We present quantitative estimations regarding the applications of controlled radiation chirp for spectroscopic applications for both incoherent and coherent detection schemes. For the coherent scheme, we expect pulse-time Fourier Transform limited spectral resolution.

## SINGLE PULSE SWEEP RESOLUTION

Since EA-FEL produces intense long pulse radiation of extremely high inherent spectral purity, it may be used for spectroscopic applications. An interesting possibility is to perform single pulse spectroscopy – namely, to use the radiation chirp as a frequency sweeper (Figure 1). Let us estimate the feasible parameters for such an application.

For spectroscopic application there are two crucial parameters: sweep range and spectral resolution. The sweep range depends on the frequency-pulling effect process. The sweep (uniform chirp) range is [1]

$$\Delta f_{sweep} = \Delta f_{hop} \frac{\Delta f_{1/2}}{\Delta f} \quad (1)$$

Where the cold resonator FWHM line width is given for a Fabri-Perot resonator (see [3]; the notation is different there) by:

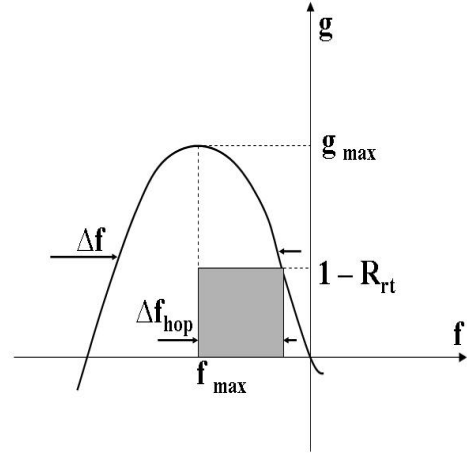


Figure 1: Frequency shift  $\Delta f_{hop}$  is the range in which the lasing condition  $g > 1 - R_{rt}$  is retained. Beyond this limit the laser would hop and lase at a different resonator mode or cease lasing altogether. This range is longer the higher the gain and the lower the loss factor  $1 - R_{rt}$ .

$$\Delta f_{1/2} = \Delta f_{FSR} \frac{(1 - R_{rt})}{2\pi} \quad (2)$$

$\Delta f_{FSR}$  is the free spectral range between the modes of the resonator, and we assumed  $1 - R_{rt} \ll 1$  ( $R_{rt}$  is the round-trip reflectivity factor of the resonator including losses and out-coupling factors). The parameter  $\Delta f_{hop}$

$$\Delta f_{hop} = f_{max} - f|_{g=1-R_{rt}} \quad (3)$$

is the range of permissible shift of the FEL gain curve during the lasing pulse during which the lasing condition  $g = (P_{out} - P_{in})/P_{in} > 1 - R_{rt}$  is retained, and beyond which the laser would hop to lase at a different resonator mode or cease lasing altogether. And the gain bandwidth is  $\Delta f$ . Clearly (see Figure 1), this range is longer the higher is the gain and the lower is the factor  $1 - R_{rt}$ . On the other hand the resonator mode line width  $\Delta f_{1/2}$  (Eq. 2) is growing in proportion to  $(1 - R_{rt})$ . Evidently there is an optimal value of  $1 - R_{rt}$  for which  $\Delta f_{sweep}$  (Eq. 1) can be maximized (in Figure 1 it corresponds to a state of maximal area of the shaded rectangle).

In Figure 2 we present the scaling of  $\Delta f_{sweep}$  as a function of the maximum gain  $g_{max}$  of the FEL, assuming operation in the low gain regime ( $g < 1$ ). The free spectral

range used was the experimentally measured  $\Delta f_{FSR} = 115\text{MHz}$ .

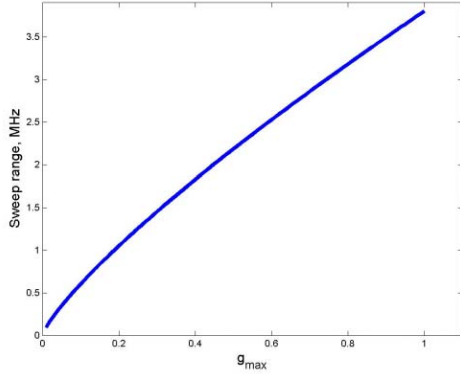


Figure 2: The scaling of  $\Delta f_{sweep}$  as function of the maximum gain  $g_{max}$  of the FEL  $g=(P_{out}-P_{in})/P_{in}$ , assuming operating in the low gain regime ( $g<1$ ). The free spectral range used was the experimental measured  $\Delta f_{FSR}=115\text{MHz}$ .

The other important parameter for spectroscopic application is the spectral resolution. Here we distinguish between coherent and incoherent detection of the chirped FEL radiation signal and the transmitted signal. In Figure 3a the detection process is described in time-frequency phase space. The center frequency of the coherent radiation pulse  $E_i(t)$  is chirped during the pulse time  $t_p$ :

$$f(t) = f_0 - f_1 t \quad (4)$$

Where  $f_1 = \Delta f_{sweep} / t_p$  is the chirp rate. The momentary spectral width of the FEL radiation is very narrow, assumed to be Fourier transform limited:

$$\Delta f_{inh} = \frac{1}{t_p} \quad (5)$$

When the FEL chirped radiation pulse is transmitted through an optical sample of complex transmission factor  $T(f)$  and the optical power is detected (incoherent detection), the time dependence of the detected power replicates the transmission spectrum of the sample  $T(f)$  (Figure 3 a, b). If we want to resolve a transmission line of width  $\delta f_{res}$  the sweep rate must be slow enough so that the sweep time through the transmission line  $\delta t = \delta f_{res} / f_1$  will be long (steady state approximation) relative to the polarization decay time  $1 / \delta f_{res}$  of the transmitted signal. This sets a limit on the spectral resolution for incoherent detection:

$$\delta f_{res} > \sqrt{f_1} = \sqrt{\frac{\Delta f_{sweep}}{t_p}} \quad (6)$$

We can take advantage of our ability to detect coherently both the FEL incoming signal and the transmitted signal using heterodyne detection as described before (Figure 3c). Having the full recorded data (amplitude and phase) of  $E_i(t)$  and  $E_o(t)$ , the full (complex) value of the transmission factor  $T(f)$  can be restored after Fourier transformation  $F\{\}$  of the recorded signals:

$$T(f) = \frac{F\{E_o(t)\}}{F\{E_i(t)\}} \quad (7)$$

The spectral resolution in this case is Fourier transform limited and given by the inherent line width value:

$$\delta f_{res} = \Delta f_{inh} = \frac{1}{t_p} \quad (8)$$

Table 1 lists resolution limits for a sweep range of 5MHz and several planned values of pulse duration for both the incoherent and coherent schemes. For coherent measurements, the resolution is limited by the inherent line width. For incoherent, it is considerably worse and scales as inverse square root of the pulse duration.

Table 1: Resolution limits for sweep range 5MHz and several pulse times.

Pulse time ( $\mu\text{s}$ )	Sweep rate $f_1=f'$ (MHz/ $\mu\text{s}$ )	Resolution $\delta f_{res}$ (kHz)	
		Coherent (complex)	Incoherent (scalar)
10	0.5	100	700
100	0.05	10	200
1000	0.005	1	70

## BROAD-BAND LOW-LOSS RESONATOR

The problem of decoupling the radiation from the electron beam with minimal losses must always be solved in an operational free electron laser. Recently we have introduced a novel wideband resonator based on combining the Talbot and confocal effects. Figure 4 describes the reconstructed Talbot image while Figure 5 describes the structure of the resonator.

The gradual improvement of the resonator of our system can be inferred from table 2.

Table 2: Gradual improvement of the Israeli free electron laser resonator quality.

Resonator Type	Total Round-Trip losses
$\Gamma$ - shape curved parallel-plate resonator	50 %
Shortened resonator (present configuration)	35 %
Rectangular Resonator with Confocal Splitter	10 %

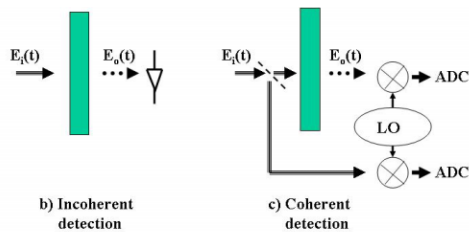
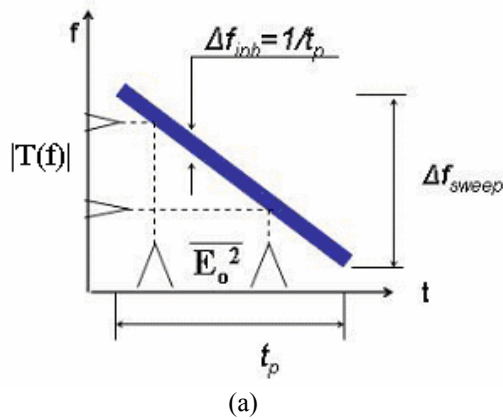


Figure 3: a) The detection process in time-frequency phase space. The center frequency of the coherent radiation pulse  $E_i(t)$  is chirped during the pulse time  $t_p$ :  $f(t) = f_0 - f_1 t$ ,  $f_1 = \Delta f_{\text{sweep}} / t_p$  is the chirp rate. b) Incoherent detection – the spectral resolution is low (see Table 1). c) Coherent detection. LO is local oscillator, ADC is analog-to-digital converter. The spectral resolution is pulse-time Fourier-limited.

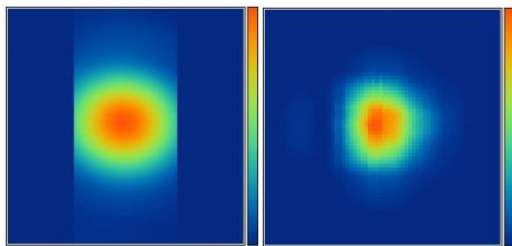


Figure 4: Field intensity distribution of the principal mode transmitted through the confocal imaging system. Input (left) and reconstructed Talbot image (right) after one pass.

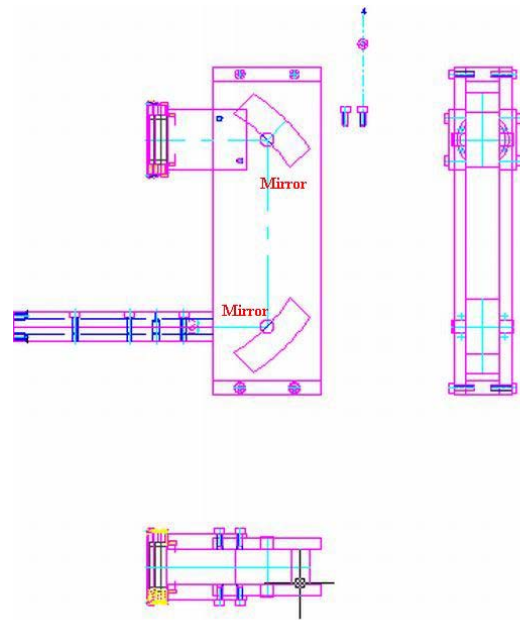


Figure 5: Confocal quasi-optical splitter layout. Two mirrors quasi-optical guiding system, placed between two parallel wave-guide structures; provide low-loss Talbot imaging operation (designed in collaboration with Gycom- Russia). Top: out-coupling system. Bottom: resonating wave-guide section, where (E-Beam – RF) interaction takes place.

### MULTI-STAGE COLLECTOR

Long pulse operation and high efficiency of EA – FEL can be obtained only if a good recovery of the spent electron beam is provided. Namely, only a small fraction of the total beam charge is lost. In order to achieve this goal, effective beam collector should be installed.

Interactions between electrons and metal can be generally divide into 2 classes:

1. Elastic events that affect the trajectories of the beam electrons within the specimen without significantly altering the energy. It results from collisions of the electron with the nuclei of the atoms, partially screened by the bound electrons.
2. Inelastic events, which result in energy transfer and produce secondary electrons.

The 2-stage collector [4] was successfully installed last year. According to EGUN simulations, its maximal energy recovery is about 28%. In addition, backscattered and secondary electrons reach the high-voltage terminal, decrease the accelerating voltage and therefore limit the pulse duration.

In order to overcome these problems, multi-stage collector (Figure 6) was constructed during the last months. It comprises of 5 electrodes housed in grounded vacuum chamber. Each electrode is set at a lower voltage than the previous. The asymmetric geometry of the collector causes the electrons to enter off-center, reducing thereby the probability of backward reflection into the

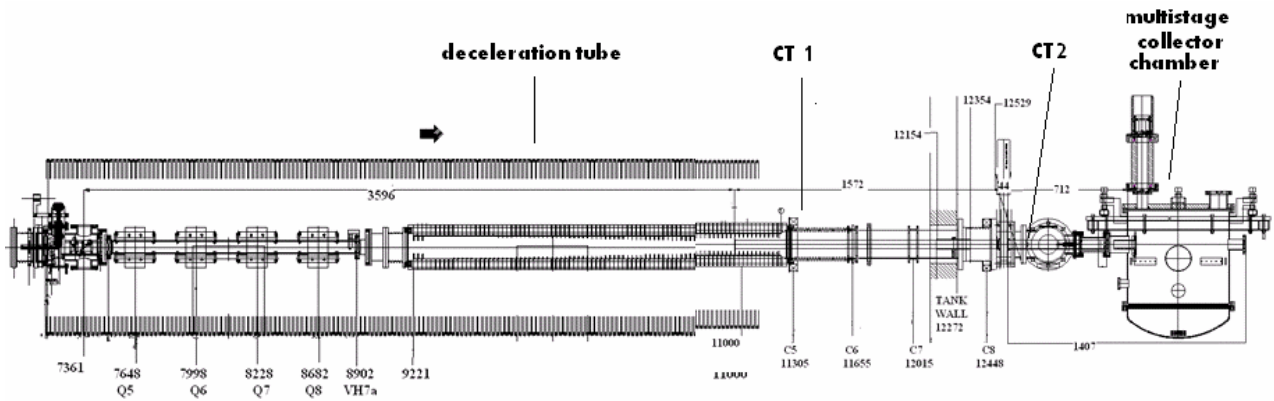


Figure 6: The multistage collector (installed during last weeks) comprises of 5 electrodes housed in grounded vacuum chamber. Each electrode is set at a lower voltage than the previous. The asymmetric geometry of the collector causes the electrons to enter off-center, reducing thereby the probability of backward reflection into the deceleration tube.

deceleration tube. Comparing with 2-stage collector, energy recovery efficiency of multi-stage collector is up to 53%, while the current recovery efficiency is 100% due to its asymmetric geometry. Table 3 summarizes the basic characteristics of the 2-stage collector vs. the multi-stage collector.

Table 3: Collector characteristics.

Collector Type	Current recovery	Energy recovery
2-stage collector	~ 98 %	28 %
Multi-stage collector	100 %	53 %

### CONCLUSIONS

The Israeli free electron laser is being upgraded towards high power and long pulse operation. The resonator was upgraded to sustain high power and reduce

losses. The collector was upgraded in order to avoid the return of electrons to the terminal and the resulting voltage drop. A stable voltage will allow long pulses and thus high resolution and high power spectroscopy. This type of characteristics are desirable for various applications such as electron spin resonance spectroscopy which of great interest to the chemical & material science community.

### REFERENCES

- [1] Y. Socol, A. Gover, A. Eliran et al. FEL'2004, Trieste, August 2004, p. 289.
- [2] R. L. Hwu, D. L. Woolard (Eds.) SPIE Proc., 5070 (2003).
- [3] A. Yariv. Optical Electronics, 3-rd ed. CBS College Publishing, 1985; §6.2-5.
- [4] M. Tecimer, M. Canter, S. Efimov et al. Nucl. Inst. Meth. In Phys. Res. A475 (2001) 574.